Lattice strain and static disorder in hydrogen-implanted and annealed single-crystal silicon as determined by large-angle convergent-beam electron diffraction

Stefano Frabboni*
Istituto Nazionale Fisica della Materia (INFM) and Dipartimento di Fisica, Università di Modena e Reggio Emilia, Via G. Campi 213/A-41100 Modena, Italy
(Received 10 July 2001; published 16 April 2002)

The large-angle convergent-beam electron-diffraction technique, available in a conventional transmission electron microscope, has been employed in order to characterize the defective layer present in heavily damaged high-dose hydrogen-implanted and low-temperature annealed ($T \leq 500\,^{\circ}C$) single-crystal silicon in terms of lattice strain and static disorder. These quantities have been measured to determine the mean relaxation volume and atomic concentration of defect clusters present in the implanted layers in order to investigate the structural features causing the reverse annealing phenomena observed in ion channeling measurements. In particular, the mean relaxation volume detected in the 300 °C 2-h annealed sample (0.1 nm^3) results in a factor three times higher than that measured in the as-implanted sample; on the contrary the mean atomic concentration of clusters does not vary appreciably after this thermal treatment. This experimental evidence suggests a nonconservative growth of clusters in the low-temperature annealing regime. After annealing at 500 °C for 2h, an increase of the relaxation volume and a significant decrease of the mean concentration is found, thus suggesting that only after this thermal treatment, producing in the meantime intrinsic defects with extended internal surfaces, defects seem to follow a conservative ripening.

DOI: 10.1103/PhysRevB.65.165436 PACS number(s): 61.14.Lj, 61.72.Tt

I. INTRODUCTION

Hydrogen in silicon has been the subject of intense study as it is known to produce defect passivation, deactivate dopants, and induce point or extended defects.[1] In high concentrations, introduced by in-diffusion[1] or by ion implantation,[2,3] hydrogen is known to produce extended planar defects (platelets), having {111} and, mainly, {100} habit planes, evolving in large "lattice cracks" observed in samples implanted at ion doses of the order of 10^{17} cm^{-2} and annealed at $T > 400\,^{\circ}C$. Platelets are then believed to trap H_2 molecules in a stressed state, building internal pressure that ultimately leads to silicon cracking. This phenomenon is the basis of a silicon-on-insulator technology known as a "smart cut."[4]

The damage evolution in samples implanted at doses up to 2×10^{16} cm^{-2} has been studied using Rutherford backscattering spectrometry and channeling (RBSC), elastic recoil detection analysis, and transmission electron microscopy (TEM).[2] It has been found that most of the interstitial-type damage created by the ion implantation process anneals out after 2 h of thermal treatment at $T = 200\,^{\circ}C$. Samples isochronal annealed at $200 < T < 400\,^{\circ}C$ for 2 h reach a quasistationary state characterized by a negligible amount of hydrogen loss. In these samples, at a depth corresponding to the hydrogen projected range, the raise of a displacement field is detected in RBSC spectra and platelets are observed in TEM images. Hydrogen effusion starts for $400 < T < 500\,^{\circ}C$, in this temperature range, the dimension and concentration of extended defects remain almost constant whereas RBSC shows an dechanneling maximum at $T = 400\,^{\circ}C$. The comparison between RBSC and TEM measurements have strongly suggested that extended defects detected by TEM were not the primary source of the observed dechanneling in the low-temperature annealed samples.[2,5] The characteristic "reverse annealing" observed in RBSC measurements has been ascribed to small clusters of H-vacancy complexes hosting H_2 molecules, too small to be observable by TEM. At present there is no structural characterization of these small defects, probably because of the experimental difficulties connected to the strong state of disorder present in the samples implanted at a high ($> 1 \times 10^{16}$ cm^{-2}) hydrogen dose.[6]

Fourier transform infrared (IR) spectroscopy experiments[7] have supported the idea of hydrogen trapping in intrinsic defects. This study has shown that isochronal annealing for T between 200 °C and 400 °C, where the amount of effused hydrogen is negligible, transforms the IR-active silanic hydrogen bonded in multivacancy defects, present in the as implanted sample, in IR-active silanic hydrogen in single vacancy complexes (VH_3 and VH_4), and IR-mute hydrogen (likely H_2). Further annealing till $T > 400\,^{\circ}C$ allows to observe IR peaks ascribed to {100} and {111} internal hydrogen terminated surfaces.

Recent theoretical studies[8] have supported all the previously reported experimental findings demonstrating that vacancies play a central role in the nucleation and growth of hydrogen-related extended defects. In particular, planar arrays of second-neighbor VH_4's seem to be the seed for both small bubbles and platelet growth, which is achieved through the formation of damage clusters involving the absorption of diffusing molecular hydrogen and emission of silicon interstitial atoms.

The structural analysis of the defective layer formed after annealing of high-dose hydrogen-implanted silicon samples seems therefore, crucial for a deep characterization of the Si(H) system.

The aim of the present paper is the study of the structural

features associated with small defects present in the defective Si(H) layers, responsible for the observed dechanneling behavior in samples annealed at temperature $T \leq 500\,^{\circ}C$. In particular, the relaxation volume and the atomic concentration of small clusters of damage will be determined. This goal will be pursued using large-angle convergent-beam electron-diffraction (LACBED) measurements of lattice strain and static disorder, as it is known that the atomic displacements produced by small clusters affect both the angular position (strain) and intensity (static disorder) of diffracted beams.[9,10]

II. SAMPLE PREPARATION AND ANALYSIS

Samples have been prepared by ion implantation of H_2^+ into single-crystal silicon. Silicon Czochralski grown disks were 6 in. in diameter, (100) oriented, and *p*-type doped with a resistivity between 30–50 Ω cm. During implantation, the sample was tiled by 7° with respect to the beam. Wafers have been implanted with H_2^+ at an energy of 31 keV with a dose of 8×10^{-15} cm^{-2}, but because of the H_2^+ fragmentation at the surface and due to the low density of collisions, this implantation is equivalent to the implantation of atomic H at a double fluence, 1.6×10^{16} cm^{-2}, and at an energy of 15.5 keV. During the implantation process the samples were kept at liquid-nitrogen temperature; after implantation some specimens underwent vacuum annealing at 300 °C and 500 °C for 2 h in order to study the thermal evolution of the crystal damage.

$[1\,\bar{1}\,0]$ TEM cross sections were prepared by mechanical dimpling, for a residual thickness of about 10 μm, and low angle ion milling with Ar^+ ions at 4 keV. TEM images were taken with a Philips EM400 operating at 100 keV. LACBED patterns have been digitally recorded in the nanoprobe mode (nominal spot size of 10 nm) by means of a 1-in. 694 Gatan charge couple device slow scan camera mounted on the same microscope. These patterns are obtained using a probe with a large convergence angle, which is focused in a plane slightly below or above the sample, thus forming a diffraction pattern (instead of an intermediate image) in the plane of the selected area aperture. This aperture is used to isolate one reflection to prevent overlapping of the diffracted beams in the final detection plane.[11] Bright field LACBED (BFLACBED) or dark field LACBED (DFLACBED) patterns can then be obtained by selecting the transmitted beam or a diffracted beam, respectively (Fig. 1). In these patterns different regions of the sample contribute to different parts of the same diffraction pattern, thus allowing an accurate comparison between the diffracted intensity coming from different areas of the sample with a spatial resolution of the order of the probe size. This peculiarity of the LACBED technique applied to TEM cross sections allowed to determine the static disorder depth profile in H, as implanted Si single-crystal samples[12] and both the size-induced tetragonal strain[13] and static disorder[14] in SiGe/Si heterostructures.

Static disorder measurements on TEM cross sections have been performed by tilting the sample of about 10° from the $[1\,\bar{1}\,0]$ zone axis around the [110] direction till the $[4\bar{4}1]$ zone axis is reached, which is a "sparse" one with sheets of

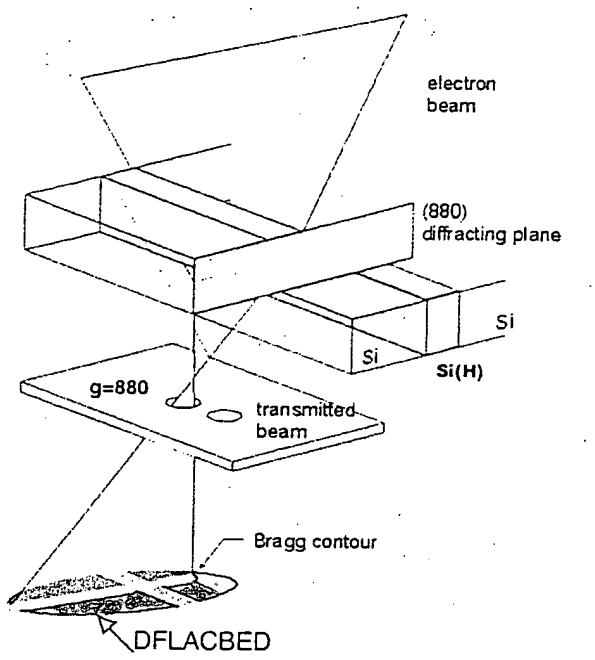

FIG. 1. Experimental LACBED geometry used in static disorder measurements. An electron beam with a very high convergence impinges on the sample oriented along the $[4\bar{4}1]$ zone axis and is focused below the specimen plane. The selected area aperture located in the corresponding plane of the microscope allow to select the (880) diffracted beam. The (880) dark field LACBED (DFLACBED) pattern is formed in the recording plane.

atomic $\{hh0\}$ planes parallel to the zone direction. Then the $g=880$ diffracted beam has been brought into the Bragg position in order to be analyzed (Fig. 1). Due to the $g\cdot r=0$ invisibility rule of the kinematical diffraction theory, the undesired effect on diffracted intensities due to sample preparation can be reasonably minimized, as $(hh0)$ reflections are perpendicular to the $[1\,\bar{1}\,0]$ direction, normal to the free surface of the TEM cross section.

Strain measurements, starting again from the $[1\,\bar{1}\,0]$ zone axis, have been performed on BFLACBED patterns obtained by tilting the specimen to about 3.5° around the [110] direction until the Bragg contour of {333} crystallographic planes crosses the defective region, avoiding intersection with the Bragg contours corresponding to different reflections (see Fig. 2).

III. LACBED STATIC DISORDER AND STRAIN DETERMINATION

A. Static disorder measurements

The information on static disorder is stored in the intensity of the diffracted beams. As it is known, the diffracted intensities for crystals with defects (i.e., for nonperiodic structures) cannot be calculated with the formulas usually adopted for the structure factors V_g of ideal crystals. However, when an average periodic lattice can be defined, the total scattered intensity distribution in a kinematical (single scattering) approximation can be written as[15]

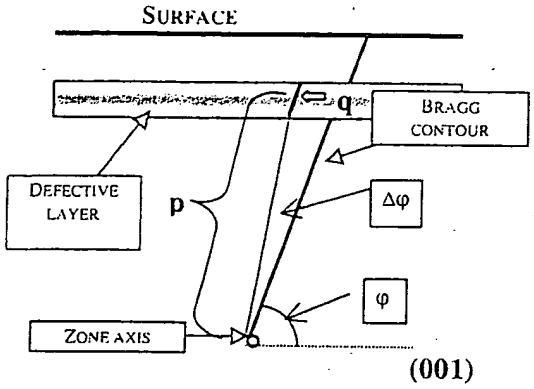

FIG. 2. Experimental geometry used for strain measurements from LACBED patterns. Using the same illumination condition of Fig. 1, but tilting the cross-sectioned sample of about 3.5° and selecting the transmitted beam with the selected area aperture, the {333} Bragg contour become visible in the pattern and superimposed to the image. The difference between the position of the Bragg contour in the silicon reference crystal and the defective layer allows to measure the strain along the direction parallel to the surface normal.

$$J_g(s)=|\langle V_g\rangle|^2+|\langle \Delta V_g(s)\rangle|^2=I_g+I_d, \qquad (1)$$

where s ($s=2\sin(\theta)/\lambda$) is the scattering vector, $|\langle V_g\rangle|^2$ is equal to the square of the gth component of the Fourier transform of the electrostatic potential $\langle V(\mathbf{r})\rangle$ of the average lattice, which produces the diffracted intensity I_g at reciprocal lattice points. The quantity $|\langle \Delta V_g(s)\rangle|^2$ is the square of the Fourier transform of the deviation from the average lattice $\langle \Delta V(r)\rangle$, which gives rise to the nonperiodic background intensity (diffuse scattering) I_d, close to the reciprocal lattice point g.

For the description of the defective layer in hydrogen-implanted silicon it seems reasonable to neglect the effect of hydrogen atoms on the electron-scattering factor; then in the simplest approach, the damage can be thought of as formed by small clusters of silicon point defects. Taking into account the relaxation of the lattice surrounding each cluster, which affects a number of atoms larger than those of the cluster itself, the decrease of Bragg intensity can be expressed by the structure factor of the crystal, V_g^{Si}, multiplied by an attenuation factor,

$$\langle V_g\rangle = V_g^{\mathrm{Si}}\exp[-L_G]. \qquad (2)$$

For clusters having a relaxation volume $\Delta\Omega_{\mathrm{cl}}$, present in an atomic concentration C_{cl}, the L_G factor is given by[9,10]

$$L_G=\sqrt{2}C_{\mathrm{cl}}g^{3/2}\frac{(|\Delta\Omega_{\mathrm{cl}}|)^{3/2}}{\Omega_{\mathrm{Si}}}, \qquad (3)$$

where g is the modulus of the reciprocal lattice vector and Ω_{Si} is the silicon atomic volume at the equilibrium density (2×10^{-2} nm^3/atom). The quantity $|\Delta\Omega_{\mathrm{cl}}|$ depends on the degree of correlation of point defects forming the cluster, being equal, in a first approximation, to the atomic volume for noncorrelated point defects and to the volume of the slipped region for dislocation loops, respectively. The simple relation between the attenuation factor L_G and the structural features of the damage reported in Eq. (3) is obtained assuming a linear superposition of the displacement field produced by each cluster present in the defective layer.[9,10] In the case of point defect clusters intermediate between noncorrelated point defects and dislocation loops, Eq. (3) is assumed as a reasonable approximation of the effect of lattice disorder on diffracted beam intensity.

In electron-diffraction experiments the reduction of the diffracted intensity due to the L_G factor cannot be predicted on the basis of a simple kinematical approximation because of the well-known many-beam (multiple-scattering) character of the electron-diffraction process. However, in a previous paper[12] it has been found that when the sample is oriented along a high indices zone axis, the ratio R between the integrated intensity in the silicon substrate, I_g^{Si}, and in damaged silicon, I_g, is given by

$$R=\frac{I_g^{\mathrm{Si}}}{I_g(L_G)}=\exp[2bL_G]. \qquad (4)$$

In particular, for the (880) diffracted beam of the $[4\bar{4}1]$ zone axis the coefficient b was found to be equal to 1.26 for 225–330 nm thickness of the sample, which is useful for LACBED experiments at 100 keV. The constant b defines the correction factor, which is applied to the logarithm of the intensity ratio reported in Eq. (4) in order to determine L_G in a "quasikinematical" approximation. Then the experimental method for disorder depth profile using DFLACBED patterns is simply based on the measurement of the profile $R(z)$ of the ratio R reported in Eq. (4), taking the integrated intensity in the silicon substrate as a reference. Once $L_G(z)$ is determined, it is possible to deduce $\Delta\Omega_{\mathrm{cl}}$ and C_{cl} if the local strain is determined.

B. Strain measurements

Local strain analyses inside the defective layer have been performed following the method proposed for Si/SiGe heterostructures,[13] which supplies a simple relationship between lattice strain and bending of Bragg contours observed in BFLACBED patterns when they cross a strained layer. Here this method is preferred to the high-order Laue zone (HOLZ) lines method used in heterostructures[14,16] because, due to the high level of static disorder present in the damaged layer, HOLZ lines become invisible, whereas the Bragg contours of medium index reflections, such as {333}, should be detectable even in disordered crystals.

In the case of ion implanted materials, a biaxial lattice strain can be present. The perpendicular strain $[\varepsilon_\perp=(a_\perp-a_{\mathrm{Si}}/a_{\mathrm{Si}})]$ evidences the change of the lattice parameter along the direction perpendicular to the surface ($a_\perp$) with respect to the undamaged substrate (a_{Si}). The parallel strain $[\varepsilon_\parallel=(a_\parallel-a_{\mathrm{Si}})/a_{\mathrm{Si}}]$ shows the variation of the in-plane lattice constant ($a_\parallel$) with respect to the silicon lattice along a direction parallel to the surface. The strain $\varepsilon_\parallel$ is present when the implanted layer undergoes plastic deformation caused by the injection of stress-relieving defects. When both $\varepsilon_\perp$ and $\varepsilon_\parallel$

are not zero, they could be measured using two independent reflections from a couple of equations such as the following:

$$(\varepsilon_\perp - \varepsilon_\parallel) = -\frac{2\Delta\varphi^{(hkl)}}{\sin 2\varphi} = -\frac{2q^{(hkl)}/p}{\sin 2\varphi}. \quad (5)$$

Here $\Delta\varphi^{(hkl)}$ is the strain induced variation of the angle φ between the (hkl) plane and the (001) interface planes, p is the angular distance from the pole corresponding to the intersection of $(hk\bar{l})$ and (hkl) contours, and $q^{(hkl)}$ is the shift of the Bragg contour (see Fig. 2).

When the $\varepsilon_\parallel$ component is negligible (an approximation frequently used in ion implanted silicon[17]) Eq. (5) applied to the {333} Bragg contour of the $[1\bar{1}0]$ cross section samples reduces to:

$$\varepsilon_\perp = -\frac{2\Delta\varphi^{(333)}}{\sin 2\varphi} = -\frac{2q^{(333)}/p}{\sin 2\varphi}. \quad (6)$$

Once $\varepsilon_\perp$ is known, the stress in the plane of the interface can be determined using the following equation:

$$\sigma = -\frac{E\nu}{1-\nu-2\nu^2}\varepsilon_\perp, \quad (7)$$

where E and ν are the Young's modulus and the Poisson's ratio, respectively. Here we assume that the isotropic elastic constant of the damaged layer are, in a first approximation, equal to those of the silicon substrate [$E = 130.2$ GPa and $\nu = 0.28$ (Ref. 18)].

In the frame of the cluster model described in the preceding section, perpendicular strain can be related to both the cluster concentration and the relaxation volume through the following relation:[9,10,17]

$$\varepsilon_\perp = \frac{1+\nu}{3(1-\nu)} C_{cl} \frac{\Delta\Omega_{cl}}{\Omega_{Si}}, \quad (8)$$

where the term $(1+\nu)/(1-\nu)$ accounts for the uniaxial geometry of the strain field.

IV. RESULTS

A. Electron microscopy

In Fig. 3 the TEM images of the analyzed samples are reported. The as implanted sample [Fig. 3(a)] shows a defective region centered at a depth of 210 nm and a width of 80 nm wide. Due to the small dimensions (diameter of 3 nm) and to the high number density ($\approx 10^{12}$ cm^{-2}) of the defects it is difficult to characterize them. Rising the annealing temperature (300 °C, 2 h), platelets (diameter of 12 nm, number density of 5×10^{11} cm^{-2}) become clearly visible [Fig. 3(b)]. Lattice images of the defective layer (not reported here) allow to measure the thickness ($\approx$1 nm) and to deduce the zigzag morphology of platelets having {111} and {100} mean habit planes. The out-of-focus images of platelets show a clear variation in contrast from underfocus to overfocus, typical of defects having an electron-optical density lower than that of the silicon matrix, thus suggesting hydrogen decoration.[2] The analysis of the defect distribution inside the defective layer shows that {111} platelets are mainly located in the deep tail of the band thus suggesting a negligible role of the implantation damage on their formation. This observation is in agreement with experimental results obtained on plasma hydrogenated silicon samples, where, in absence of implantation damage, {111} platelets form.[19] On the contrary, {100} platelets are detected mainly in the central part of the defective layer where the radiation damage and the hydrogen profiles mainly intersect. Dimensions and concentration of platelets are in agreement with literature data on the study of the growth kinetics at 450 °C for 1–15 min in samples implanted at room temperature at a dose of few 10^{16} cm^{-2} that have shown a conservative ripening (Ostwald ripening) of

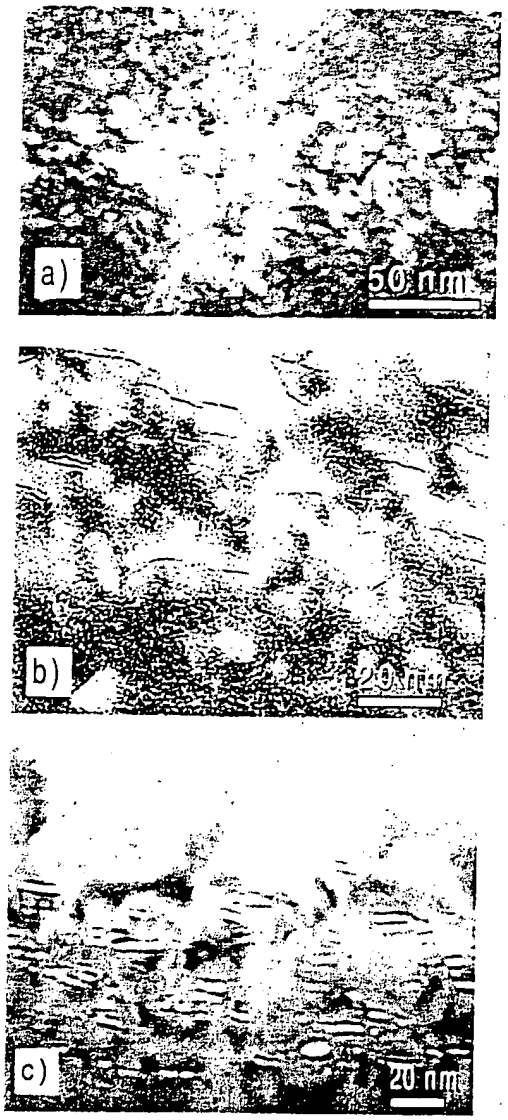

FIG. 3. Cross section TEM images of the analyzed samples. (a) Dark field ($g=004$) image of the as implanted sample. (b) Out-of-focus image of the 300 °C 2 h annealed sample. {111} and {100}: platelets are visible. (c) Out-of-focus image of the 500 °C 2 h annealed sample. Some "microcracks" with {111} and {100} facets are detected.

the extended defects.[20] In Fig. 1(c) the TEM cross-section image of the 500 °C annealed sample is reported; extended defects have lateral dimensions and a number density similar to those observed in the 300 °C annealed samples but show {100} and {111} faceted cores. On the basis of this TEM evidence platelets observed after 300 °C annealing are distinguished from defects observed in the 500 °C annealed sample, hereafter called "microcracks."

B. LACBED static disorder and strain measurements

In Fig. 4(a) is reported a (880) DFLACBED, aside of the as-implanted sample image in order to compare the intensity of the Bragg contour with the morphology of the sample. The diffracted intensity decreases when it reaches the defective region and presents a minimum approximately at the depth where the image shows the center of the defective band (210 nm).[12]

The static disorder increase, which follows the annealing, is qualitatively observed by comparing the DFLACBED pattern of the sample annealed at 300 °C [Fig. 4(d)] to the as implanted one, as the (880) Bragg contour loses almost completely its intensity in the damaged region of the annealed sample. An appreciable recovery of crystal quality is detected in the sample annealed at 500 °C [Fig. 4(f)]. The raise of the static disorder strength from the as implanted sample to the 300 °C annealed one can be better analyzed if the depth profiles of the integrated intensity ratio $R(z)$ of Eq. (4) measured in the three analyzed samples are compared. It must be pointed out that in the defective layer of the annealed samples of the present study, due to the high level of static disorder, the diffracted beams loose a large part of their intensity and high diffuse scattering is observed near the Bragg position. For this region, we have tried to improve the process to give a more reliable method of disorder depth profiling proposed in Ref. 12, thereby extending it to the case of highly damaged samples. The procedure proposed here differs from the previous one in two aspects: first, the integrated intensity profile is directly obtained from the DFLACBED patterns and not from the envelope of single rocking curves. Second the background subtraction is performed using depth profiles of integrated diffuse intensity and not using a linear background subtraction on each rocking curve. In Fig. 5 the steps followed in order to obtain the depth profile of the integrated intensity are reported.

(i) Directly from the DFLACBED [Fig. 5(a)] three integrated intensity profiles are obtained. The first one, $P1$, allows to obtain the raw integrated intensity profile of the Bragg contour [Fig. 5(b)]. The profiles $P2$ [Fig. 5(c)] and $P3$ [Fig. 5(d)] are used to perform the background subtraction.

(ii) Profiles $P2$ and $P3$ are averaged [Fig. 5(e)] in order to approximately evaluate the integrated background under the Bragg peak. In principle, this point is the most critical one but seems reasonable because, as expected for point defects and clusters,[21] the peak of the diffuse scattering is asymmetric and not coincident with the Bragg one.

(iii) The average profile obtained in step (ii) is subtracted to $P1$ in order to obtain the background subtracted integrated intensity depth profile $I_g(z)$ [Fig. 5(f)].

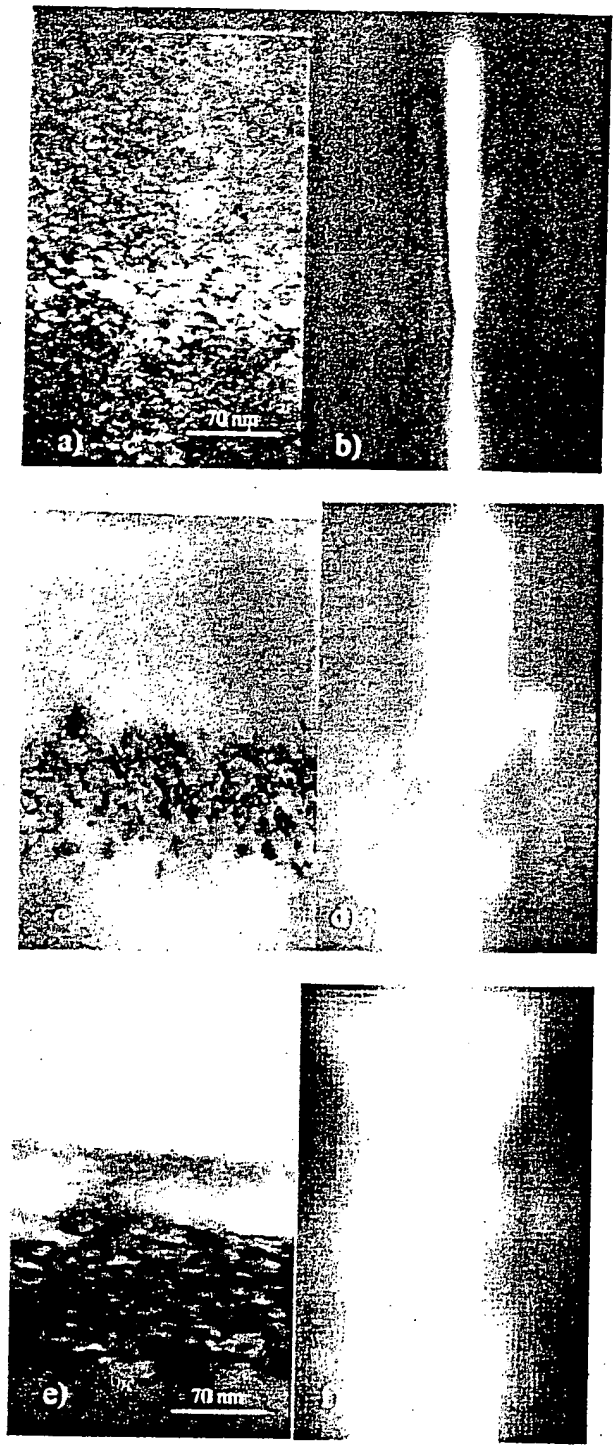

FIG. 4. Cross section TEM images and (880) DFLACBED patterns of the as implanted sample (a), (b); 300 °C 2 h annealed sample (c), (d); and 500 °C 2 h annealed sample (e), (f). The images allow to calibrate the depth scale of the DFLACBED patterns.

In Fig. 6 are reported the $R(z)$ plots obtained by applying Eq. (4) to the integrated intensity profiles after background

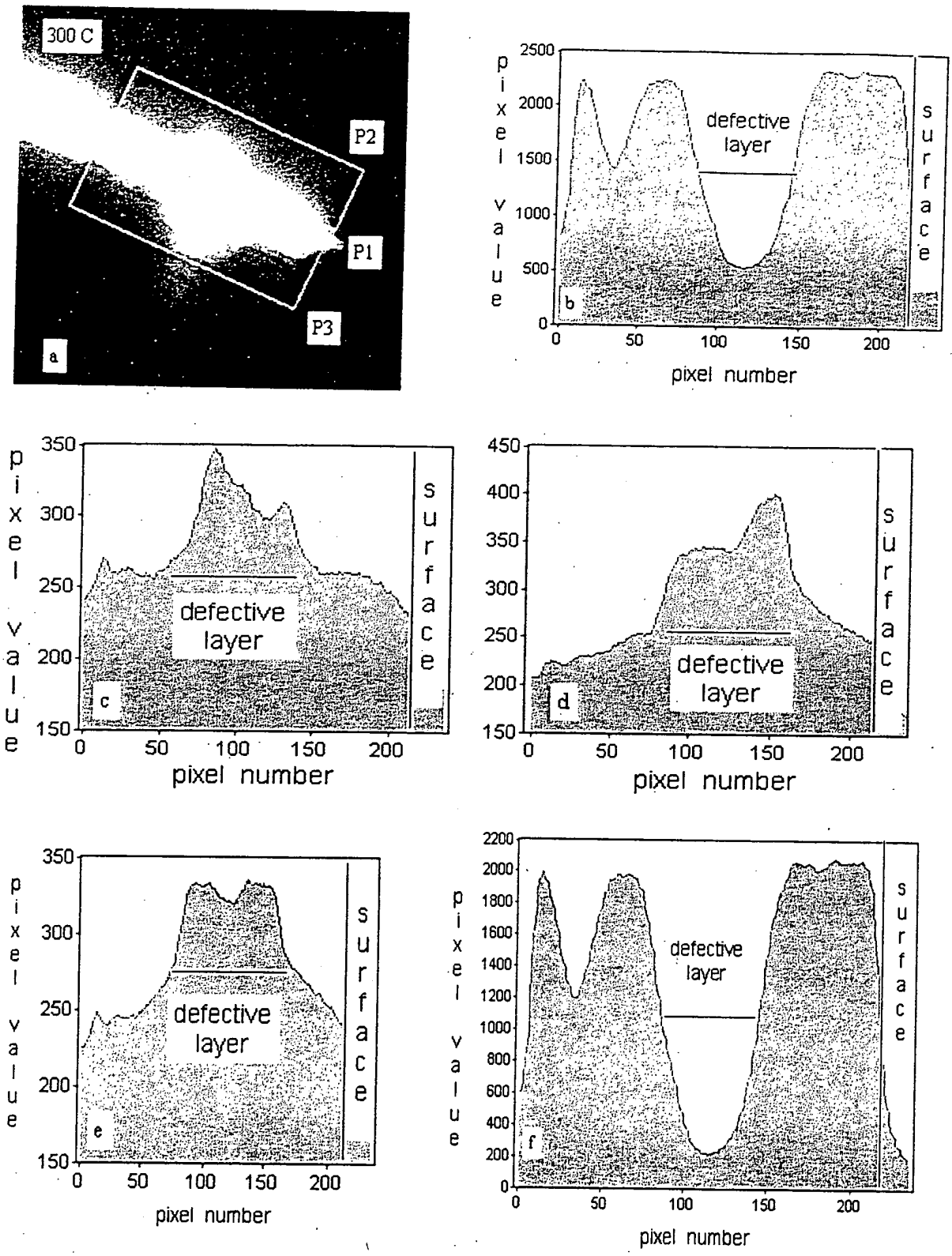

FIG. 5. Procedure adopted in order to obtain the depth profile of the integrated intensity (intensity). (a) DFLACBED pattern of the 300 °C 2 h annealed sample. The rectangular masks correspond to the integration field of the rocking curve, near the Bragg peak ($P1$), and in the diffuse scattering region close to the Bragg peak ($P2$) and ($P3$). (b) Raw diffracted intensity profile, $P1$. (c) Diffuse intensity profile, $P2$. (d) Diffuse intensity profile, $P3$. (e) Average diffuse intensity profile. (f) Background subtracted intensity profile.

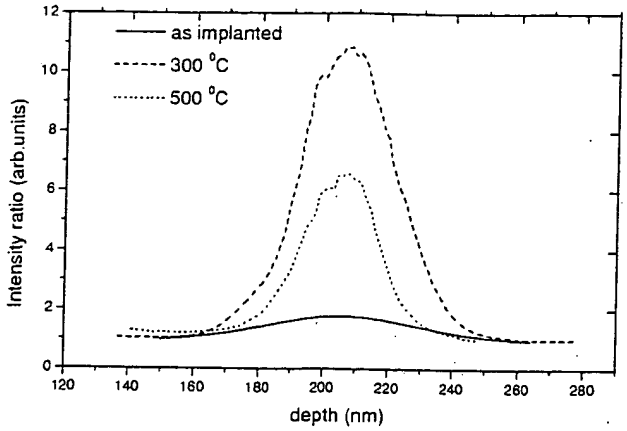

FIG. 6. Depth profile of the ratio between the integrated intensity in the defective layer and in the silicon substrate as a function of the annealing temperature.

subtraction and calibration of the depth scale. Now the quantitative comparison between the crystal quality of three samples can be easily done.

Strain measurements have been performed using the LACBED technique in the BFLACBED geometry (see Sec. III B). In order to quantify the perpendicular strain $\varepsilon_\perp$ the angular shift q of the Bragg contour corresponding to the {333} crystallographic planes inside the defective layer is determined. Actually, due to the well-known relaxation of stresses in cross-sectioned samples, the angular shift q comes out from the unrelaxed part of the strain field. This systematic error is of the order of 15% in ⟨110⟩ cross sections[16] and is taken into account in the evaluation of the error bar of the strain values. In Fig. 7(a) the experimental LACBED pattern of the 300 °C annealed sample that allows to measure the shift of the (333) reflection inside the damage region is shown. Due to the strong static disorder the Bragg contour is barely visible in the image. In Fig. 7(b) an edge-filtered image of the {333} Bragg contour of Fig. 7(a) is reported, showing slightly better the angular shift of the Bragg contour inside the damaged region. In Fig. 7(c) line scans across the {333} reflection are reported, near the middle of the damage layer, showing well-defined minima that have been used to measure the angular shift q from the silicon Bragg position (reported for comparison). The angular shift of the {333} reflection in the 500 °C annealed sample is indistinguishable from the as-implanted one and is omitted in the plot. In Table I the mean values of both the perpendicular strain and the related in-plane stress are reported showing the high stress (compressive, about 3 GPa) present in the defective layer of the 300 °C annealed sample. A more accurate analysis of the stress/strain profile was impossible because of the inclined position of the {333} Bragg contour with respect to the damage layer, which worsens the spatial resolution.

V. DISCUSSION

From a TEM point of view, platelets (clearly visible in the 300 °C annealed sample) seem to be the relevant extended defects formed after low-temperature annealing. After annealing at $T = 500$ °C these defects evolve towards "microcracks," i.e., faceted intrinsic defects with a nonequilibrium shape when, as reported in the literature,[2,3,7] H starts to desorb from the sample. Electron-diffraction measurements of strain and static disorder show a "reverse annealing." In particular, the 300 °C annealed sample appears more stressed and disordered than the other samples. These evidences are in qualitative agreement with previously reported x-ray double crystal diffraction DCD (Ref. 6) and RBSC (Ref. 2) measurements performed on similar samples. In particular, strain and static disorder measured by DCD and LACBED

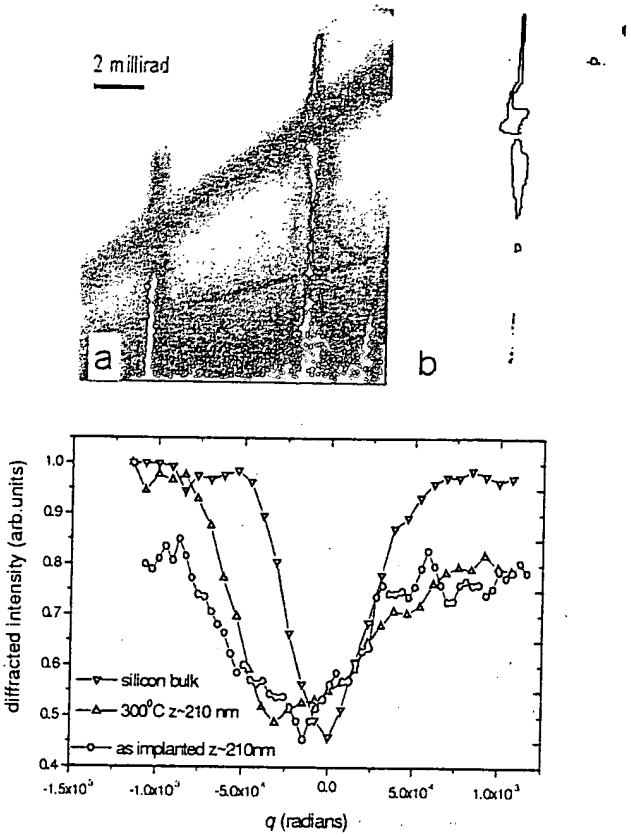

FIG. 7. (a) BFLACBED taken in the 300 °C annealed sample for the strain measurement. The {333} and {444} Bragg contour are vertical and inclined of about 54° with respect to the surface. The bending of the Bragg contour inside the defective layer is visible. (b) Edge filtered image of the {333} Bragg contour to make more evident the angular shift of the Bragg contour in the defective layer. (c) Intensity profiles across the {333} Bragg contour used for strain measurement in the analyzed samples.

TABLE I. Mean perpendicular strain and in-plane stress values obtained from LACBED measurements in the three analyzed samples

	As *implanted*	300 °C	500 °C
$\varepsilon_\perp$ (10^{-3})	$.5 \pm 1$	12 ± 2	5 ± 1
σ (GPa)	-1 ± 0.1	-3 ± 0.2	-1 ± 0.1

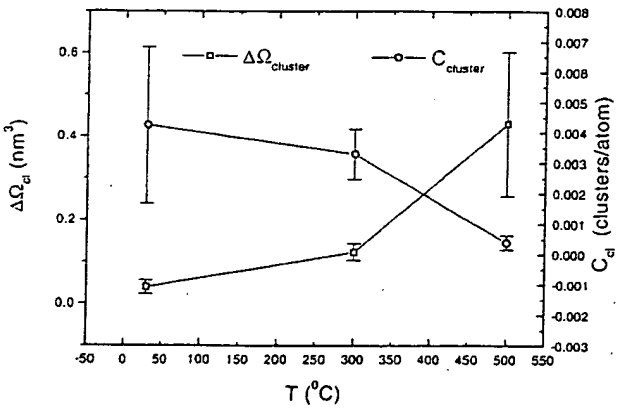

FIG. 8. Plot of the mean relaxation volume and of the mean concentration of clusters as a function of the annealing temperature. The values are deduced by combining strain and static disorder results.

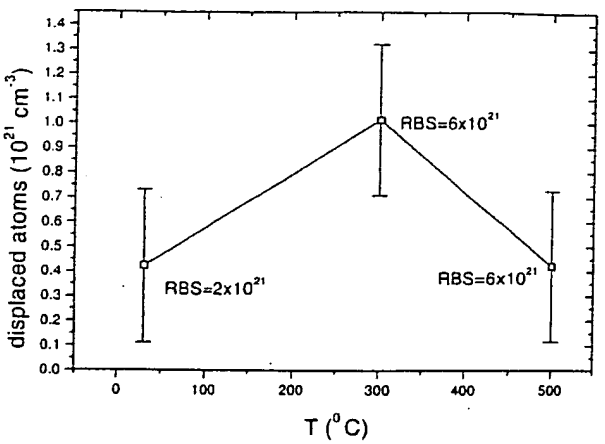

FIG. 9. Comparison between the concentration of displaced atoms expressed in numbers of "interstitial equivalent point defect" as determined by LACBED and RBS ch.

are, in an isotropic approximation, almost directly comparable as diffraction techniques are mainly sensitive to the long-range displacement fields produced by defects. The agreement is satisfactory in as-implanted and 500 °C annealed samples, where DCD measurements show the presence of a perpendicular strain almost constant inside the defective layer [ranging from $(5-7)\times10^{-3}$] and the highest value of static disorder in the annealed sample. Slightly different is the situation in the 300 °C annealed sample, where BFLACBED measurements show a perpendicular strain value higher than 10^{-2}, which has no counterpart in DCD measurements probably because the peak of static disorder is so high that, for x-ray measurements, the presence of an amorphous buried layer at the depth of about 210 nm cannot be excluded.[6] On the contrary, from electron-diffraction and high-resolution TEM (not reported here) point of view, this sample appears still crystalline, but characterized by a high level of static disorder and a measurable strain. Strain and static disorder data allow to exploit the cluster model reported in Sec. III for the quantitative structural interpretation of electron-diffraction measurements in terms of cluster mean relaxation volume and cluster concentration [see Eqn. (3) and Eqn. (8)]. In Fig. (8) the results obtained by applying the cluster model to the data measured near the peak of the damage are summarized. According to strain measurements, the mean relaxation volume is positive, but always higher than that expected in the case of interstitial point defects ($\Delta\Omega_I = 1.8\times10^{-2}$ nm^3 $=0.9\,\Omega_{Si}$[22]). Taking the data from the as-implanted sample as a reference for comparison among the samples, it is found that the mean relaxation volume increases by a factor 3 in the 300 °C annealed sample and by an order of magnitude after annealing at 500 °C. On the contrary the cluster concentration does not change significantly upon the first annealing step and only after annealing at $T=500$ °C it markedly decreases. It can be further observed that the relaxation volume (cluster concentration) determined by DFLACBED is always lower (higher) than the corresponding quantities deduced from extended defects observed by TEM.[2] These evidences support the idea that the extended defects represent only a small fraction of the total damage distribution, whereas hydrogen-related point defect clusters grow upon low-temperature annealing. In addition, the increase of the relaxation volume at constant cluster concentration observed after annealing at 300 °C suggests a nonconservative growth of the damage during this thermal treatment. Then the experimental evidences reported in Fig. 8 could be the structural fingerprint of the progressive segregation of H_2 molecules in hydrogen decorated vacancies, which, following a recently proposed model,[8] sustain the growth of second-neighbor VH_4's with the emission of interstitial defects, thus generating very complex clusters of damage. If this attribution is correct, these clusters could have a relaxation volume of about 0.1 nm^3. The additional relaxation volume increase and the significant cluster concentration decrease observed after 500 °C annealing agree with the model of conservative growth of damage observed for extended defects in samples annealed at 450 °C.[20]

In order to proceed in the comparison among electron-diffraction measurements and results obtained with different techniques on the same samples, it has been tried to compare the electron-diffraction data, obtained from the cluster model, to RBSC results. Differently from the case of diffraction (electron or x-ray) techniques, this comparison could be performed if electron-diffraction and ion techniques both convert "raw" data (strain and static disorder for electron diffraction and dechanneling yield for RBSC) in comparable quantities using models of damage. A quite common interpretation of RBSC data is to convert dechanneling yield depth profiles in "interstitial equivalent" displaced atoms profiles (see, e.g., Ref. 2). The same parameter can be obtained from electron-diffraction data, by simply multiplying the cluster relaxation volume, the cluster concentration, and the silicon atomic density (5×10^{22} atoms/cm^3) and normalizing to the single interstitial relaxation volume. Here the additional assumption with respect to the cluster model reported in Sec. III A is that not only the displacement field produced by each cluster, but also the displacement field produced by each atom in the cluster superimpose linearly. In Fig. 9 are reported the defect concentrations measured by

DFLACBED near the damage peak as a function of the annealing temperature. The trend is found in fair agreement with the RBSC data reported in the literature[2] thus supporting the "nonconservative" growth of damage in the low-temperature annealed sample. The agreement in the absolute values of the defect concentration is not satisfactory, particularly in the 500 °C sample where the dimension of defects make the hypothesis of linear superposition of the displacement field inside each cluster not applicable.

VI. CONCLUSIONS

In this paper the TEM/LACBED techniques have been applied to characterize the defective layer in hydrogen-implanted single-crystal silicon. It has been shown that the LACBED technique is able to measure strain and static disorder in heavily damaged crystals, allowing to determine the mean relaxation volume and the mean concentration of clusters present in the defective layer. It is found that for samples annealed at $T=300\,^{\circ}C$ for 2 h platelets (about 12 nm long and 1 nm thick) form, but smaller clusters of point defects exist in larger concentration, as the mean relaxation volume of defects is of the order of 0.1 nm^3. In this sample the cluster mean relaxation volume is higher than that measured in the as-implanted sample, whereas the mean concentration of defects does not vary appreciably. An additional increase of the relaxation volume and a significant decrease of the number density of clusters is found after annealing at 500 °C for 2 h. These evidences indicate that only after this thermal treatment, responsible in the mean time for the hydrogen effusion from the surface and for the formation of "microcracks," defects seem to start the surface reconstruction and the conservative ripening, which, in samples implanted at a higher hydrogen dose, is the base of the "smart-cut" technological process.

ACKNOWLEDGMENTS

This work was partially supported by an MIUR grant (NATI Program). The author is indebted to G. Ottaviani and to G. F. Cerofolini for stimulating discussion on the Si(H) system.

*Email address: frabboni@unimo.it

[1] *Hydrogen in Semiconductors*, edited by J. I. Pankove and N. M. Johnson, Semiconductors and Semimetals Vol. 34 (Academic, Boston, 1991).

[2] G. F. Cerofolini, L. Meda, R. Balboni, F. Corni, S. Frabboni, G. Ottaviani, R. Tonini, M. Anderle, and R. Canteri, Phys. Rev. B **46**, 2061 (1992).

[3] G. F. Cerofolini, F. Corni, S. Frabboni, C. Nobili, G. Ottaviani, and R. Tonini, Mater. Sci. Eng., R. **237**, 1 (2000).

[4] M. Bruel, Electron. Lett. **31**, 1201 (1995).

[5] G. F. Cerofolini, R. Balboni, D. Bisero, F. Corni, S. Frabboni, G. Ottaviani, R. Tonini, R. S. Brusa, A. Zecca, M. Ceschini, G. Giebel, and L. Pavesi, Phys. Status Solidi A **150**, 539 (1995).

[6] D. Bisero, F. Corni, S. Frabboni, R. Tonini, and G. Ottaviani, R. Balboni, J. Appl. Phys. **83**, 4106 (1998).

[7] M. K. Weldon, V. E. Marsico, Y. J. Chabal, A. Agarwal, D. J. Eaglesham, J. Sapjeta, W. L. Brown, D. C. Jacobson, Y. Caudano, S. B. Christman, and E. E. Chaban, J. Vac. Sci. Technol. B **15**, 1065 (1997).

[8] F. A. Reboredo, M. Ferconi, and S. T. Pantelides, Phys. Rev. Lett. **82**, 4870 (1999).

[9] P. H. Dederichs, Phys. Rev. B **1**, 1306 (1970).

[10] P. H. Dederichs, J. Phys. F: Met. Phys. **3**, 471 (1973).

[11] M. Tanaka, J. Electron Microsc. **35**, 314 (1986).

[12] S. Frabboni and F. Gambetta, Phys. Rev. Lett. **81**, 3155 (1998).

[13] X. F. Duan, D. Cherns, and W. Steeds, Philos. Mag. A **70**, 1091 (1994).

[14] S. Frabboni, F. Gambetta, A. Armigliato, R. Balboni, S. Balboni, and F. Cembali, Phys. Rev. B **60**, 13 750 (1999).

[15] J. M. Cowley, *Diffraction Physics* (North-Holland, Amsterdam, 1990).

[16] R. Balboni, S. Frabboni, and A. Armigliato, Philos. Mag. A **77**, 67 (1998).

[17] M. Servidori, Nucl. Instrum. Methods Phys. Res. B **19/20**, 443 (1987).

[18] W. A. Brantley, J. Appl. Phys. **44**, 534 (1973).

[19] S. J. Jeng, G. S. Oehrlein, and G. J. Scilla, Appl. Phys. Lett. **53**, 1735 (1988).

[20] J. Grisolia, G. Ben. Assayag, A. Claverie, B. Aspar, C. Lagahe, and L. Laanab, Appl. Phys. Lett. **76**, 852 (2000).

[21] K. Nordlund, P. Partyca, R. S. Averback, I. K. Robinson, and P. Ehrhart, J. Appl. Phys. **88**, 2278 (2000).

[22] M. Tang, L. Colombo, J. Zhu, and T. Diaz de la Rubia, Phys. Rev. B **55**, 14 279 (1997).